Electronic Supplementary Material (ESI) for Journal of Materials Chemistry A.

Supporting Information

Foldable Chromium Vanadate Cathodes for High-Performance Aqueous Zinc Ion Batteries

Peiqi Shi[a,b,#], Meng Huang[a,b,#], Lianmeng Cui[a], Bomian Zhang[a,b], Lei Zhang[a,b], Qinyou An[a,b,*], Liqiang Mai[a,b,*]

[a] State Key Laboratory of Advanced Technology for Materials Synthesis and Processing, Wuhan University of Technology, Wuhan, 430070, P.R. China

[b] The Sanya Science and Education Innovation Park, Wuhan University of Technology, Sanya, 572000, P.R. China.

[#]These authors contributed equally to this work

[*]Corresponding Author: Qinyou An, E-mail: anqinyou86@whut.edu.cn; Liqiang Mai, E-mail: mlq518@whut.edu.cn

Electrochemical Measurements

In electrochemical measurement, 2032 coin cells were prepared in air by Zn foil as anode electrode, glass fiber as separator and 4 M $Zn(CF_3SO_3)_2$ as the electrolyte. In the preparation of the cathode electrode, 70% of the active substances (CVO, CVO/CNT, and CVO/CNT-rGO), 20% of the super P, and 10% of the PVDF binder were mixed into N-Methyl-2-pyrrolidone (NMP), then the uniform slurry was coated on carbon paper, the electrodes were then dried in a vacuum oven 70℃ for 24h. The mass loading range of electrode is 1 to 2 mg cm^{-2}. Then, NEWARE battery testing system (CT-4008T-5V10mA-164, Shenzhen, China) within the potential windows of 0.2-1.8 V was used to evaluate the electrochemical performances. And LAND battery testing system (CT2001A, Wuhan, China) was used to test Zn^{2+} ion diffusion coefficient. While the cyclic voltammetry (CV) and electrochemical impedance spectroscopy (EIS) measurements were tested by an electrochemical workstation (CHI760E and Autolab PGSTAT 302 N) at room temperature. The GITT test was performed at a current density of 0.05 A g^{-1}, a relaxation time (τ) of 60 min, and a recording interval of 30 s.

The LAND and NEWARE battery testing system and electrochemical workstation with high sensitivity and accuracy have been in our laboratory, which can help us obtain the required electrochemical performance data in this research.

Material Characterization

X-ray diffraction (XRD) measurement was measured using a Bruker D8 Discover X-ray diffractometer with the non-monochromatic Cu Kα X-ray as the source (λ = 1.5406 Å). Inductively coupled plasma (ICP) measurement was recorded with a PerkinElmer Optima 4300DV spectrometer. Raman spectra were obtained using a HORIBA LabRAM HR Evolution & SmartSPM spectroscopy system with an excitation laser wavelength of λ = 532 nm. Thermogravimetric analysis (TGA) curves were conducted by using a Netzsch STA 449C simultaneous analyzer. Fourier transform infrared (FTIR) spectra were performed using a Nicolet 6700 (Thermo Fisher Scientific Co., USA) IR spectrometer. The Brunauer-Emmett-Teller (BET) surface area was collected through Tristar II 3020 instrument at 77 K. Scanning electron microscopy (SEM) images were carried out on a JSM-7100F scanning electron microscope. Transmission electron microscopy (TEM) and high-resolution TEM (HRTEM) images were obtained with a JEM-1400Plus STEM/EDS microscope. X-ray photoelectron spectroscopy (XPS) spectra were conducted with a Shimadzu AXIS SUPRA.

These experimental instruments have been in our laboratory, which can not only meet the material characterization analysis required by this research, but also save time and cost.

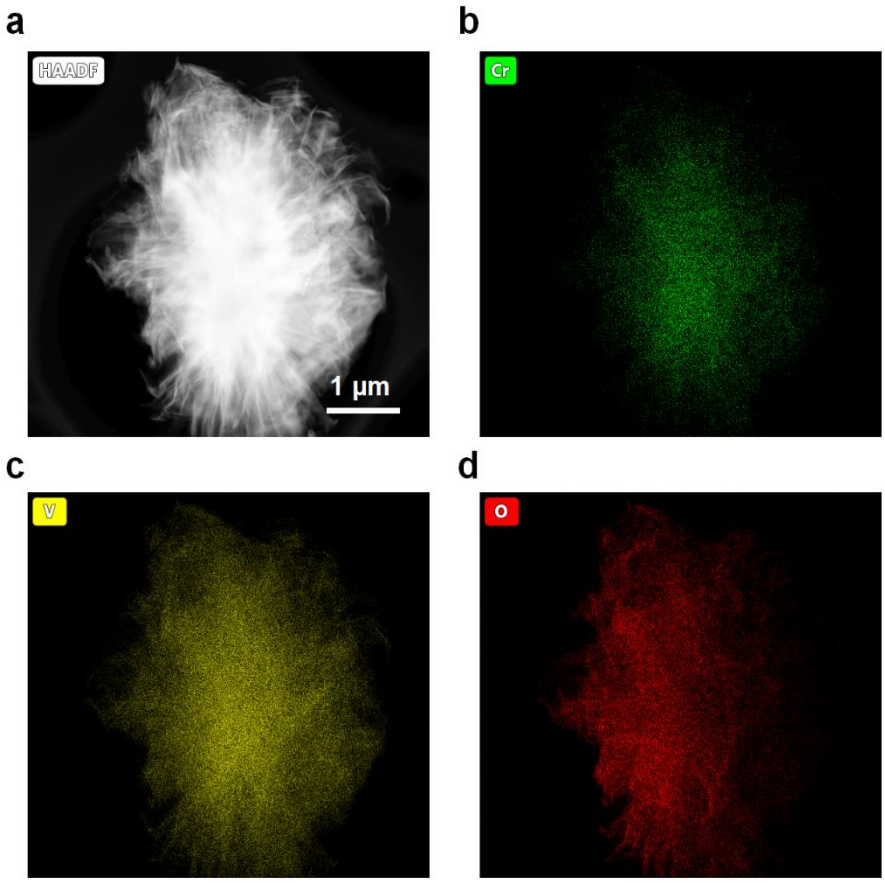

Fig. S1 (a) HAADF image of the CVO; (b-d) Corresponding elemental maps of the CVO.

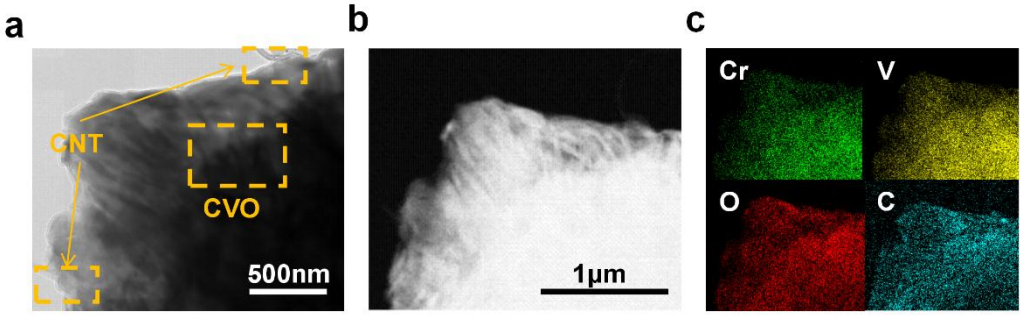

Fig. S2 (a) TEM image of CVO/CNT;(b) HAADF image of CVO/CNT; (c)Corresponding elemental maps of CVO/CNT.

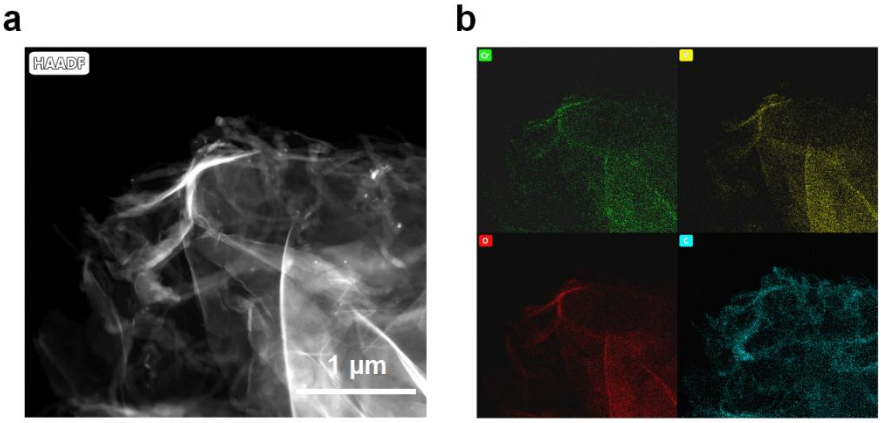

Fig. S3 (a) HAADF image of the CVO/CNT-rGO; (b) Corresponding elemental maps of the CVO.

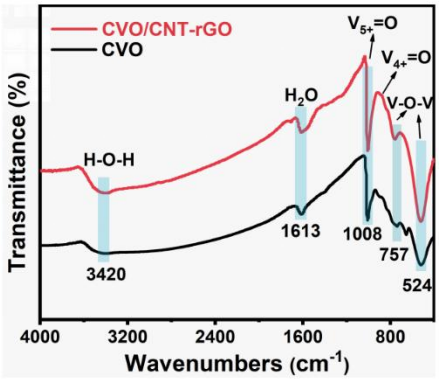

Fig. S4 FTIR spectra of the CVO and CVO/CNT-rGO.

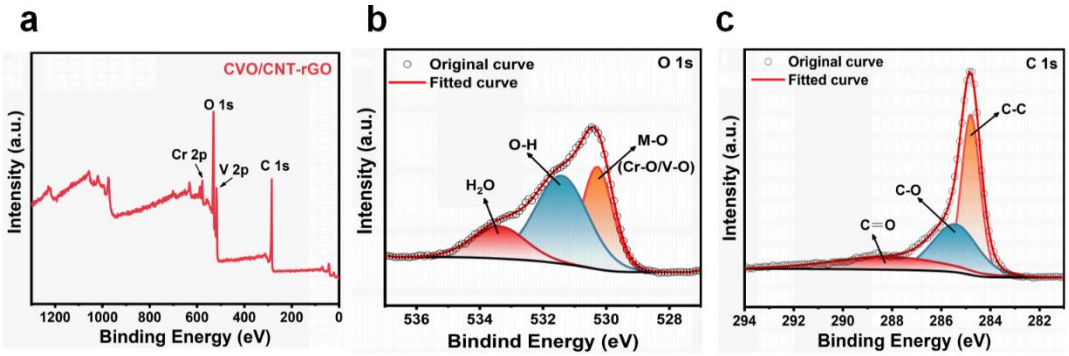

Fig. S5 (a) XPS spectra of CVO/CNT-rGO; (b) XPS spectra of O 1s; (c) XPS spectra of C 1s.

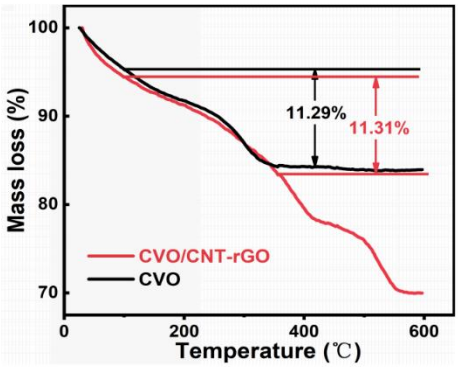

Fig. S6 TGA curves of CVO and CVO/CNT-rGO sample under air atmosphere.

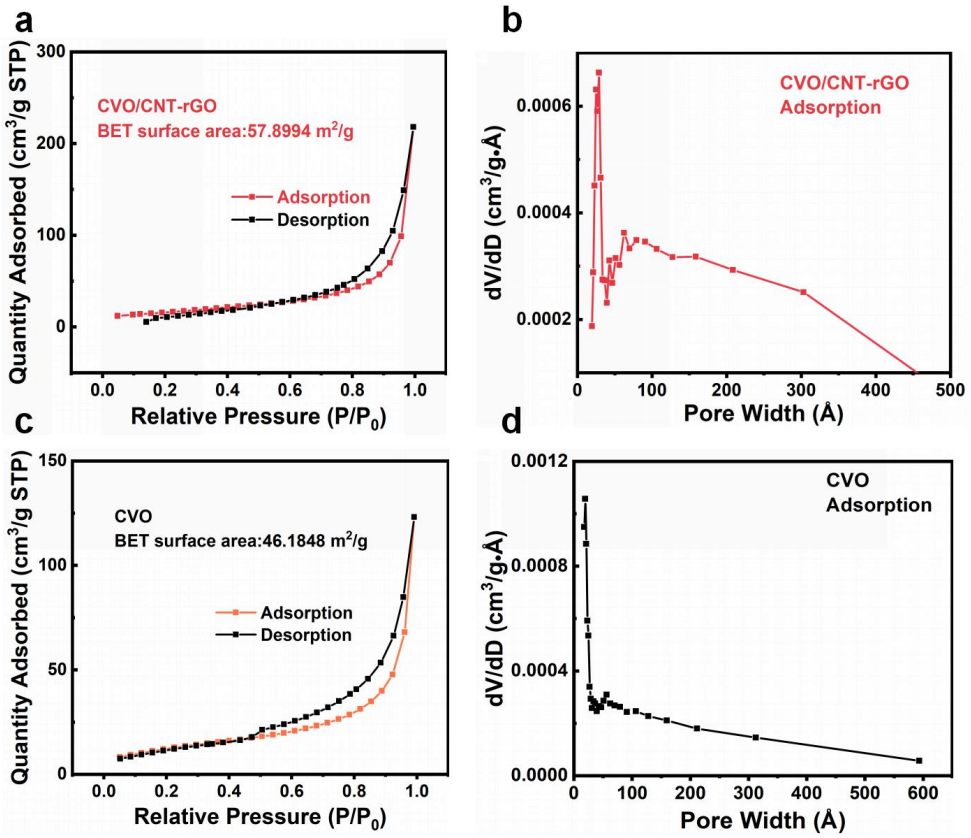

Fig. S7 (a) Nitrogen adsorption–desorption isotherm of the CVO/CNT-rGO; (b) The pore size distribution of CVO/CNT-rGO; (c) Nitrogen adsorption–desorption isotherm of the CVO; (d) The pore size distribution of CVO.

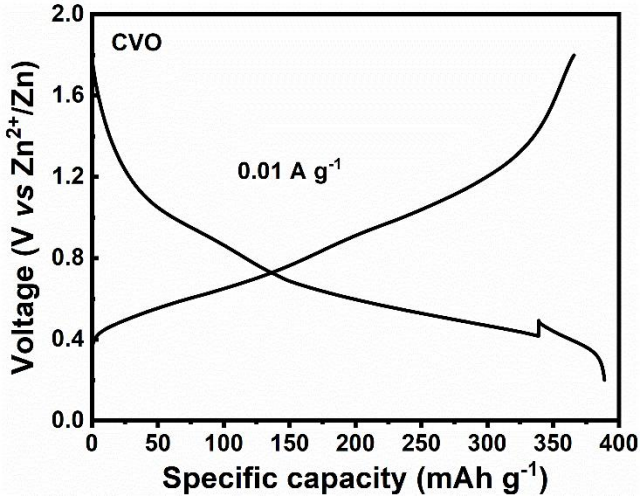

Fig. S8 Galvanostatic charge-discharge curves of CVO at 0.01 A g^{-1}.

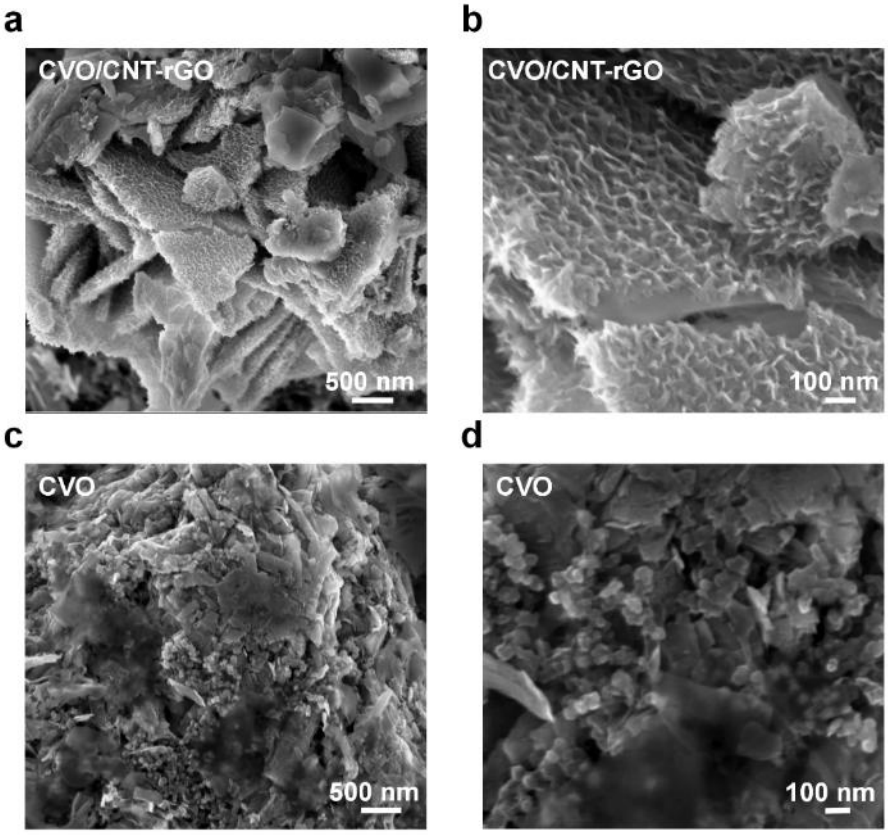

Fig. S9 (a-b) SEM image of CVO/CNT-rGO electrode after 1000 cycles as the cathode. (c-d) SEM image of CVO electrode after 1000 cycles as the cathode.

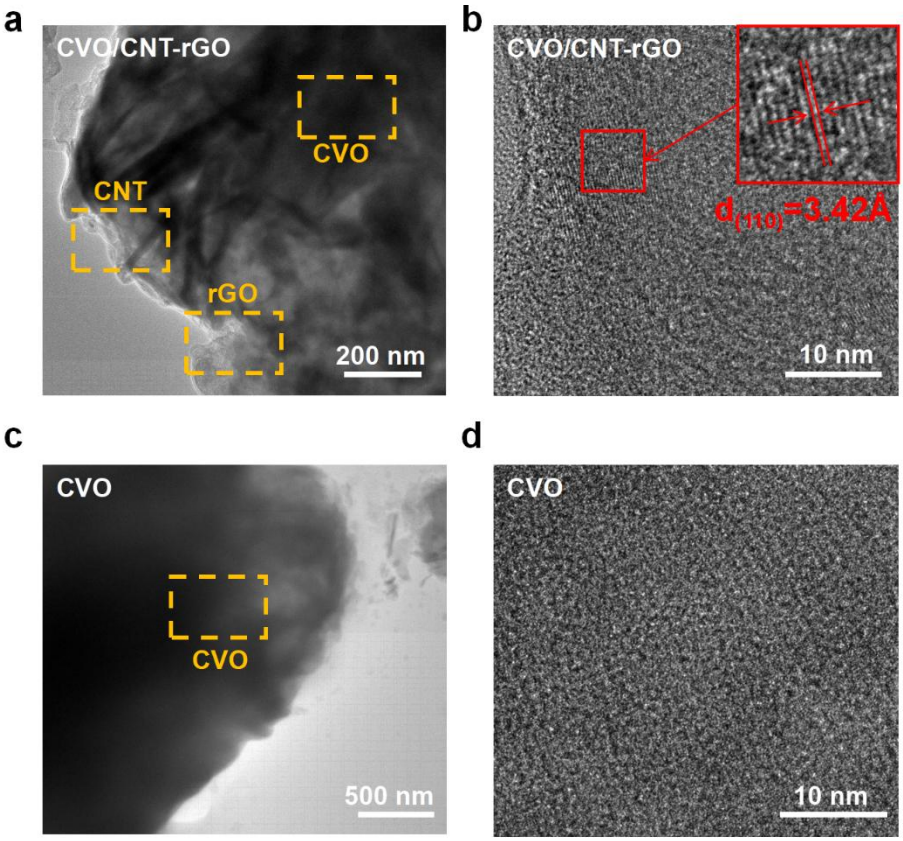

Fig. S10 (a) TEM image of CVO/CNT-rGO electrode after 1000 cycles. (b) HRTEM image of CVO/CNT-rGO electrode after 1000 cycles. (c)TEM image of CVO electrode after 1000 cycles. (d) HRTEM image of CVO electrode after 1000 cycles.

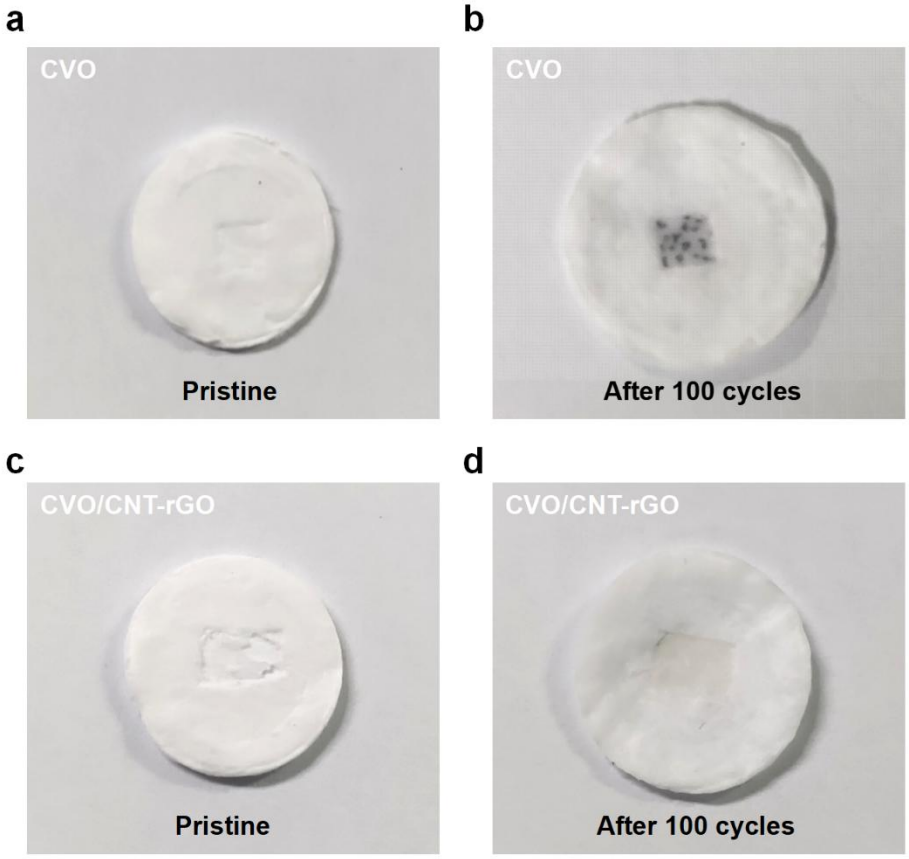

Fig. S11 (a) Pristine separator and (b) separator after 100 cycles of the CVO. (c) Pristine separator and (d) separator after 100 cycles of the CVO/CNT-rGO.

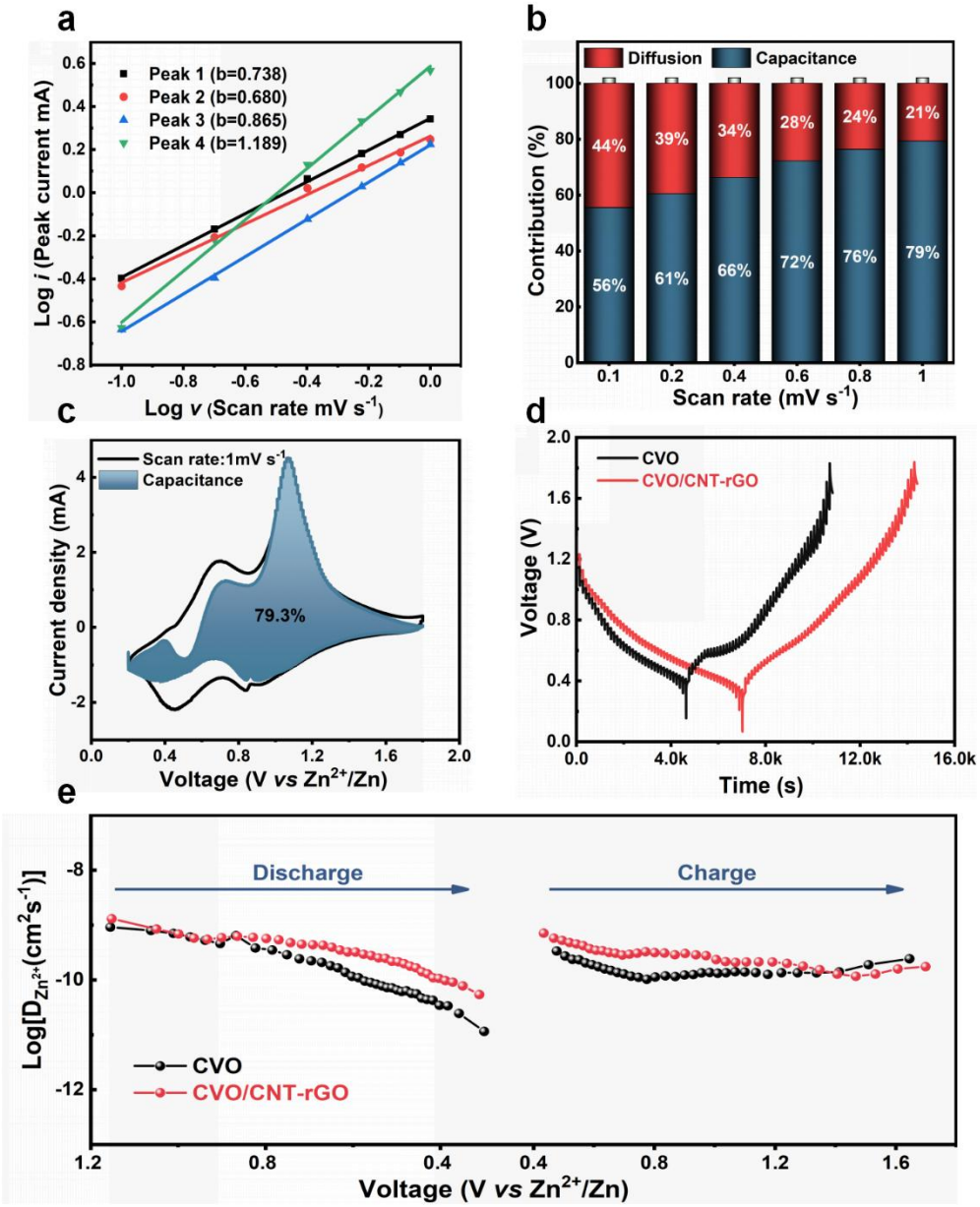

Fig. S12 (a) Log(*i*) versus log(*v*) plots of four redox peaks in CV curves; (b) Pseudocapacitance contribution of CVO/CNT-rGO at various scan rates; (c) Capacitive contribution of CVO/CNT-rGO at 1 mV s^{-1}; (d) The GITT curves of the CVO and CVO/CNT-rGO at 0.05 A g^{-1}; (e) Zn^{2+} diffusion coefficients (D_{Zn}^{2+}) comparison between CVO and CVO/CNT-rGO.

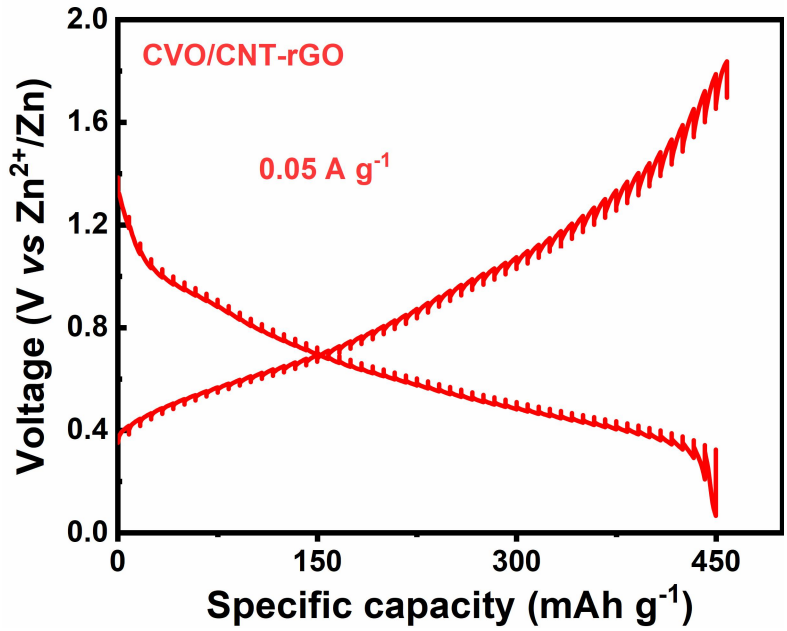

Fig. S13 The GITT curves of the CVO/CNT-rGO at 0.05 A g^{-1}.

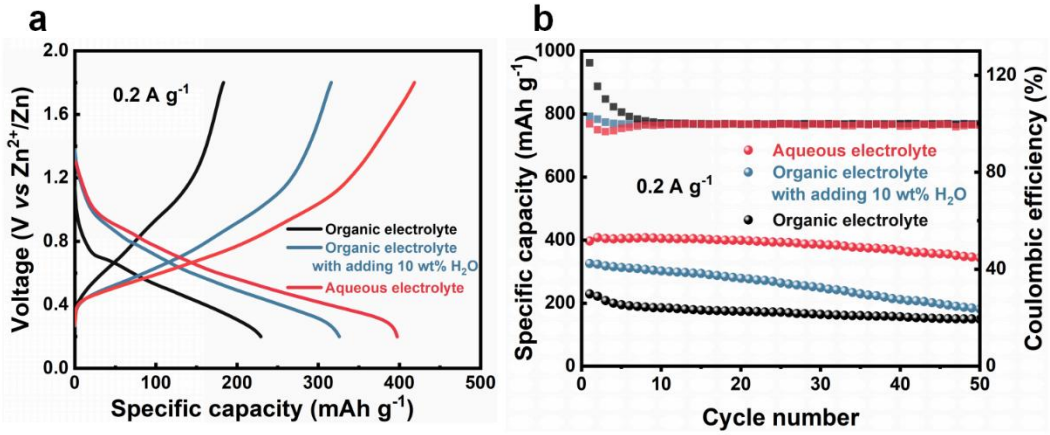

Fig. S14 (a) Comparison of typical charge/discharge curves of CVO/CNT-rGO electrode in different electrolytes; (b) Comparison of cycling performance of CVO/CNT-rGO electrode in different electrolytes.

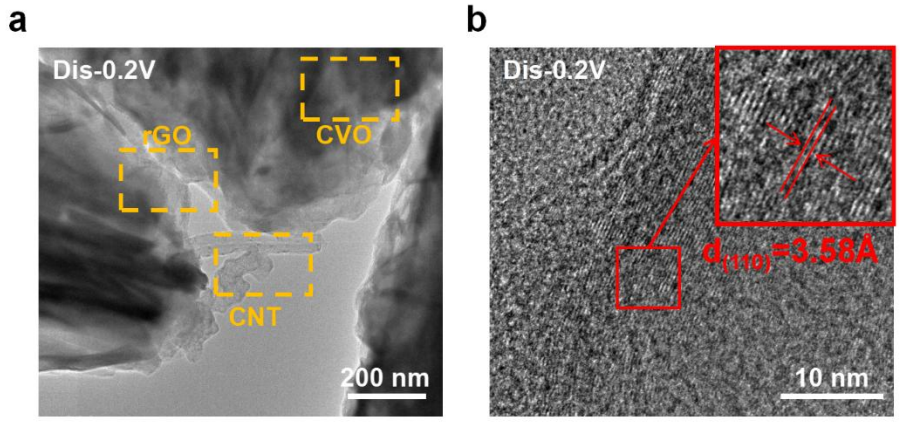

Fig. S15 (a) TEM image of CVO/CNT-rGO during the first discharging cycle. (b)HRTEM image of CVO/CNT-rGO during the first discharging cycle.

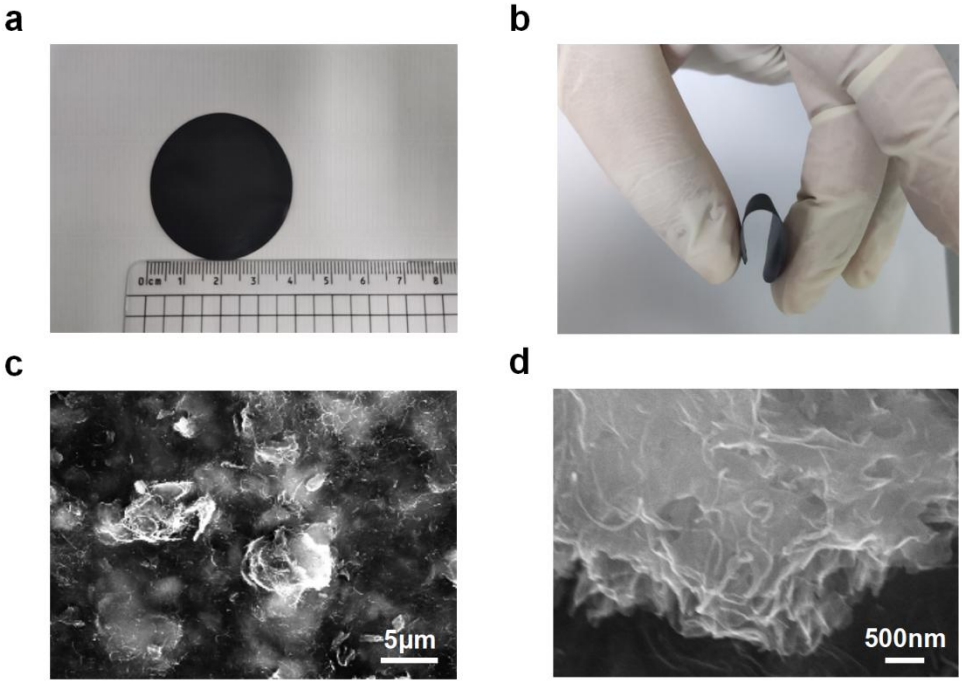

Fig. S16 (a) The film of CVO/CNT-rGO; (b) The bending capacity of the film; (c-d) SEM images of the film of the CVO/CNT-rGO.

Table S1 The ICP results of the CVO.

ICP		Cr	V
CVO	Mass percent	11.6075 %	30.6506 %
	Molar ratio	1	2.7

Table S2 The Organic element analysis (C/H/O/N/S) results of the CVO.

		C	H	O	N
CVO	Mass percent	0.16 %	1.923 %	25.893 %	0.06 %
	Molar ratio	/	1	0.84	/

Table S3 The stoichiometry ratio of the CVO ($Cr_xV_yO_z \cdot nH_2O$).

Sample	x	y	z	n
CVO	1	2.7	4.36	2.85

Table S4 Comparison of CVO/CNT-rGO with the vanadium-based cathode materials in AZIBs.

Materials	Specific capacity	Cycle number	Capacity retention	Reference
$Na_{0.33}V_2O_5$	250 mAh g^{-1} at 0.2A g^{-1}	1000 (1 A g^{-1})	93%	1
$Zn_{0.25}V_2O_5 \cdot nH_2O$	282 mAh g^{-1} at 0.3 A g^{-1}	1000 (2.4 A g^{-1})	80.0%	2
CuVOH@CC	217.8mAh g^{-1} at 0.1 A g^{-1}	2000 (1 A g^{-1})	53.8%	3
KMgVOH	408 mAhg^{-1} at 0.1A g^{-1}	2000 (4 A g^{-1})	72.0%	4
bilayer-VOP	313.6 mAh g^{-1} at 0.1 A g^{-1}	2000 (5 A g^{-1})	76.8%	5
$MnV_{12}O_{31} \cdot 10H_2O$	433 mAh g^{-1} at 0.1 A g^{-1}	5000 (3 A g^{-1})	81.47%	6
CrVO3	188.8 mAh g^{-1} at 0.5 A g^{-1}	1000 (4 A g^{-1})	76%	7
$Zn_3V_3O_8$	285 mAh g^{-1} at 0.1 A g^{-1}	2000 (5 A g^{-1})	72.6%	8
ZnO@VOH	365 mAh g^{-1} at 0.5 A g^{-1}	1000 (5 A g^{-1})	71%	9
$Ca_{0.67}V_8O_{20} \cdot 3.5H_2O$	466 mAh g^{-1} at 0.1 A g^{-1}	2000 (5 A g^{-1})	74%	10
$Fe_5V_{15}O_{39}(OH)_9 \cdot 9H_2O$	385 mAh g^{-1} at 0.1 A g^{-1}	500 (5 A g^{-1})	> 80%	11
$K_2V_6O_{16} \cdot 2.7H_2O$	237 mAh g^{-1} at 0.5 A g^{-1}	500 (6 A g^{-1})	82%	12
MnVO	415 mAhg^{-1} at 0.05 A g^{-1}	2000 (4 A g^{-1})	92%	13
VS_2	190.3 mAh g^{-1} at 0.05 A g^{-1}	200 (0.5 A g^{-1})	98%	14
VO_2@V_2C	190 mAh g^{-1} at 0.2 A g^{-1}	1000 (5 A g^{-1})	81%	15
$V_6O_{13} \cdot nH_2O$	395 mAh g^{-1} at 0.1 A g^{-1}	1000 (5 A g^{-1})	87%	16
AlVOH/rGO	384 mAh g^{-1} at 0.1 A g^{-1}	1300 (4 A g^{-1})	-	17

CVO/CNT-rGO	397.3 mAh g^{-1} at 0.1 A g^{-1}	1000 (5 A g^{-1})	87%	**This work**

Reference

1 P. He, G. Zhang, X. Liao, M. Yan, X. Xu, Q. An, J. Liu and L. Mai, *Adv. Energy Mater.*, 2018, **8**, 1702463.

2 D. Kundu, B. D. Adams, V. Duffort, S. H. Vajargah and L. F. Nazar, *Nat. Energy*, 2016, **1**, 16119.

3 J. Ren, P. Hong, Y. Ran, Y. Chen, X. Xiao and Y. Wang, *Inorg. Chem. Front.*, 2022, **9**, 792-804.

4 Z. Feng, Y. Zhang, J. Sun, Y. Liu, H. Jiang, M. Cui, T. Hu and C. Meng, *Chem. Eng. J.*, 2022, **433**, 133795.

5 Z. Wu, C. Lu, F. Ye, L. Zhang, L. Jiang, Q. Liu, H. Dong, Z. Sun and L. Hu, *Adv. Funct. Mater.*, 2021, **31**, 2106816.

6 Y. Ran, J. Ren, Z. C. Yang, H. Zhao, Y. Wang and Y. Lei, *Small Structures*, 2023, **4**, 2300136.

7 Y. Bai, H. Zhang, B. Xiang, Y. Zhou, L. Dou and G. Dong, *J. Colloid Interface Sci.*, 2021, **597**, 422-428.

8 J. Wu, Q. Kuang, K. Zhang, J. Feng, C. Huang, J. Li, Q. Fan, Y. Dong and Y. Zhao, *Energy Stor. Mater.*, 2021, **41**, 297-309.

9 B. Shuai, C. Zhou, Y. Pi and X. Xu, *ACS Appl. Energy Mater.*, 2022, **5**, 6139-6145.

10 K. Zhu, T. Wu and K. Huang, *ACS Nano*, 2019, **13**, 14447-14458.

11 Z. Peng, Q. Wei, S. Tan, P. He, W. Luo, Q. An and L. Mai, *ChemComm.*, 2018, **54**, 4041-4044.

12 B. Sambandam, V. Soundharrajan, S. Kim, M. H. Alfaruqi, J. Jo, S. Kim, V. Mathew, Y.-k. Sun and J. Kim, *J. Mater. Chem. A*, 2018, **6**, 15530-15539.

13 C. Liu, Z. Neale, J. Zheng, X. Jia, J. Huang, M. Yan, M. Tian, M. Wang, J. Yang and G. Cao, *Energy Environ.Sci.*, 2019, **12**, 2273-2285.

14 P. He, M. Yan, G. Zhang, R. Sun, L. Chen, Q. An and L. Mai, *Adv. Energy Mater.*, 2017, **7**, 1601920.

15 J. Chen, B. Xiao, C. Hu, H. Chen, J. Huang, D. Yan and S. Peng, *ACS Appl. Mater. Interfaces*, 2022, **14**, 28760-28768.

16 J. Lai, H. Zhu, X. Zhu, H. Koritala and Y. Wang, *ACS Appl. Energy Mater.*, 2019, **2**, 1988-1996.

17 Z. Feng, Y. Zhang, X. Yu, Y. Yu, C. Huang and C. Meng, *Colloids Surf. A Physicochem. Eng. Asp.*, 2022, **641**, 128473.